Nov 9th, 12:00 AM - 12:00 AM

Effect of Web Perforation on the Behaviour of Cold-Formed Steel C-Shape Slender Column Subjected to Non-Uniform Cross-Sectional Distribution of Elevated Temperatures

S. Yang

L. Xu

Wei-Wen Yu International Specialty Conference on Cold-Formed Steel Structures
Baltimore, Maryland, U.S.A, November 9 & 10, 2016

Effect of Web Perforation on the Behaviour of Cold-formed Steel C-shape Slender Column Subjected to Non-uniform Cross-sectional Distribution of Elevated Temperature

S. Yang[1] and L. Xu[2]

Abstract

Presented in this paper is a numerical investigation on the effect of web perforations on the behaviour of cold-formed steel C-shape columns subjected to non-uniform cross-sectional distribution of elevated temperature with use of finite element analysis. The length of web perforation investigated varies from 0 mm to 630 mm (25 in.). The non-uniform cross-sectional distributions of elevated temperatures are obtained from finite element thermal analysis of insulated CFS walls subjected to standard fire up to 105 minutes. Sequentially coupled thermal-stress analyses were carried out under a transient state condition. The concentrically loaded cold-formed steel C-shape columns with load ratios of 0.6, 0.7, 0.8 and 0.9 are investigated. Initial global geometrical imperfection is accounted for in the. It is found that the column failed by global buckling about its weak axis together with the local failure around the region of the web perforation at mid-height of the column and thermal bowing towards the fire-exposed side. The obtained results from the finite element analysis demonstrate that the web perforation has an influence on the temperature distribution of the cross-section of the C-shape column, but the temperature gradient within a cross-section is hardly associated with length of the web perforation. As a result, the differences of failure times among the cold-formed steel C-shape columns with different lengths of web perforation subjected to a same load ratio are found to be within 10%.

1. Introduction

Used as wall studs, cold-formed steel (CFS) C-shape columns are often enclosed with insulation in the wall cavity and protected by gypsum boards on both sides, in CFS wall assemblies. Pre-punched web perforations of the column accommodate the passage of utilities and installation intermediate braces in practice. A CFS C-shape column in a CFS wall assembly is subjected to non-uniform cross-sectional distribution of elevated temperature when the wall

[1]Research Assistant: Department of Civil and Environmental Engineering, University of Waterloo, ON, Canada
[2]Corresponding author, Professor: Department of Civil and Environmental Engineering, University of Waterloo, ON, Canada; E-mail: lxu@uwaterloo.ca

assembly is exposed to fire attack from one side. Several experimental investigations were carried out to study the behavior of CFS C-shape columns subjected to local buckling [1, 2, 5], distortional buckling [3] and flexural-torsional buckling [4] subjected to uniform cross-sectional distribution of elevated temperature. The CFS C-shape columns tested in the foregoing investigations had no web perforations, except that in [1, 5]. The results from [1, 5] show that the web perforations can alter the failure modes of short columns at temperatures above 400 ºC, whereas it has little influence on the load capacity of the column. Experimental investigations on the behaviour of CFS C-shape columns subjected to non-uniform cross-sectional distribution of elevated temperature are commonly carried out by full-scale fire tests of CFS wall assemblies, which are costly and time-consuming. Finite element analysis (FEA), as an alternative approach, has been used to study the behavior of CFS C-columns at non-uniform cross-sectional elevated temperature by other researchers [6-9]. However, little study is available on CFS C-shape columns with web perforations subjected to non-uniform elevated temperatures. This study aims to investigate the effect of web perforations on the behaviour of CFS C-shape slender columns subjected to non-uniform cross-sectional distribution of elevated temperatures with use of finite element analysis. Sequentially coupled thermal-stress analyses were carried out under a transient state condition. The non-uniform cross-sectional distributions of elevated temperature are obtained from the thermal analysis of insulated CFS walls. CFS C-shape slender columns subjected to the concentrically axial load with different ratios are investigated. The material properties of CFS at elevated temperatures and initial geometrical imperfections are considered in the investigation.

2. Finite element analysis

2.1 FE model and sequentially coupled thermal-stress analyses

Illustrated in Figure 1 are the cross-section of CFS wall segment modelled in FEA and the nominal cross-sectional dimensions of CFS C-shape column at the location of web perforation. The modelled CFS wall segment, 600 mm (24 in.) in width and 3200 mm (126 in.) in height, consists of a CFS C-shape column (150 mm ×40 mm×15 mm×1.5 mm) sheathed with a double layer of 12 mm thick gypsum board on both sides. The 150 mm deep wall cavities are filled with glass fibre. Five web perforations are evenly spaced 640 mm o.c. along the height of the column. The length of web perforation varies from 0 mm to 630 mm (25 in.), whereas the width of the perforation remains as a constant of 38 mm (1.5 in.). Six different lengths of perforation (L_h), i.e., 0 mm (0 in.), 130 mm (5 in.), 250 mm (10 in.), 380 mm (15 in.), 510 mm (20 in.) and 630 mm (25 in.) are investigated in this study.

The finite element program ABAQUS [10] is used in this study. The FEA procedure commenced a thermal analysis to obtain the non-uniform cross-sectional distributions of elevated temperature of a CFS column from a 600mm wide CFS wall section and followed by a structural analysis to investigate the behaviour of the column at the elevated temperature. The nodal temperatures at the elevated temperature obtained from the thermal analysis were applied as a predefined boundary condition of the FE model in the structural analysis.

2.2 FE thermal analysis

Finite element thermal analysis was performed for insulated CFS walls subjected to standard fire. The method used to develop the FE thermal model in this study is similar to that from [8] which was verified and calibrated with experimental tests. The gypsum boards and glass fibre are modeled using 8-node continuum solid elements (DC3D8). The CFS C-shape column is simulated with 4-node shell elements (DS4). No thermal contact resistance between adjacent elements is assumed. Double layers of gypsum board and glass fibre are merged into one instance, whereas the thermal properties of each material are defined accordingly. The thermal properties of glass fibre, gypsum board and steel, including thermal conductivity, specific heat, and density, are adopted from those reported in [11]. The temperature degree of freedom of the contact nodes between gypsum board and column flanges on both sides and that between glass fibre and column web are tied. In the tie constraints specified in ABAQUS, the nodes of gypsum board and glass fibre instance act as master nodes whereas the nodes associated with column are defined as slave ones. Figure 2 illustrates the FE meshes of the CFS wall segment. Heat transfer through solid materials is by means of conduction. On the fire-exposed and unexposed sides, the heat transmission is described as a combined action of radiation and convection. A convection coefficient of h=25 W/m^{2}K and 10 W/m^{2}K is used on the fire-exposed side and the unexposed side, respectively. Relative emissivity is taken as 0.9 for gypsum board surface. The CFS walls are exposed to the standard fire curve defined by ISO 834 [12] for up to 105 minutes. The ambient temperature is assumed to be 20 ^{o}C.

Figure 3 shows the predicted temperatures in the CFS wall and C-shape column at 105 minutes' fire exposure. The temperature of the gypsum board surface is 1023 ^{o}C on the fire-exposed side (ES), and 66 ^{o}C on the unexposed side (UES). It can be seen that non-uniform cross-sectional distribution of elevated temperature in the CFS C-shape column also varies along the height of the column. The maximum temperature in the column is no more than 654 ^{o}C. The cross-sectional views on Section 1 and 2 illustrate the temperature contours at the location without and with web perforation, respectively. It is observed that

the temperature of Section 2 is higher on the hot flange and lower on the cold flange comparing with the corresponding temperatures of Section 1. The web temperature distribution of Section 2 is also different from that of Section 1 due to the presence of the perforation.

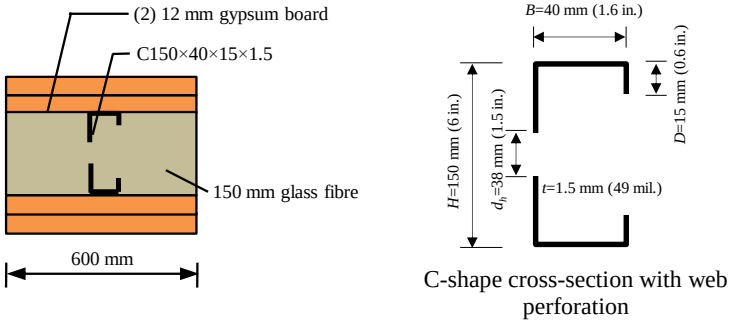

Figure 1 Configuration of CFS wall section

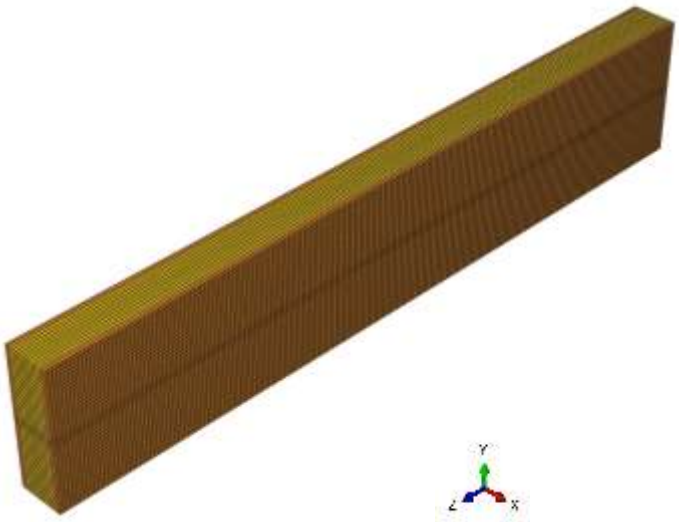

Figure 2 Finite element mesh of CFS wall segment

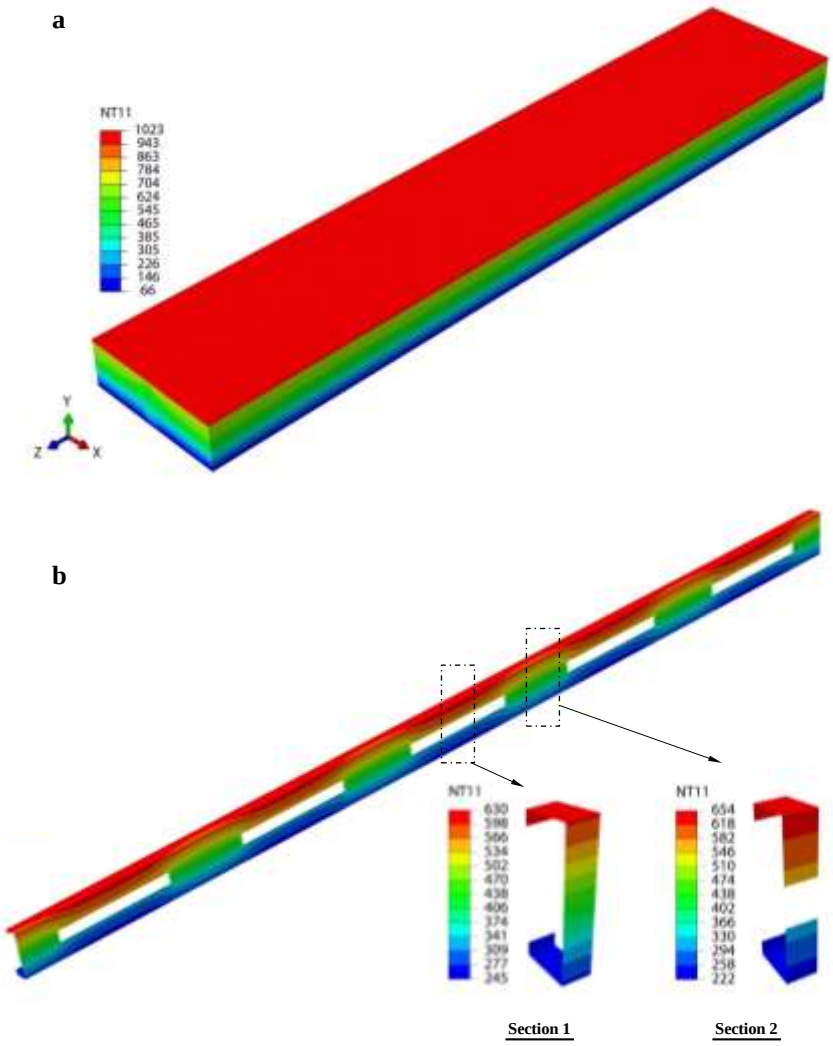

Figure 3 Temperature contour (L_h =380 mm): (a) CFS wall and (b) C-shape column.

2.3 FE structural analysis

The FE structural analysis was performed under a transient state condition in two steps. At first, a pre-determined axial compression load was applied as the

Step 1. After that, the temperature distributions obtained from the heat transfer analysis was incorporated in the analysis as the Step-2.

In the structural analysis, the CFS C-shape column is modeled with a rigid plate (150 mm×40 mm) attached to each end as shown in Figure 5. The reference point of the rigid plate coincides with the centroid of the cross-section of the column. The element type and mesh of the CFS C-shape column is the same as those of the heat transfer model, for which correlations are required to import the temperature from the heat transfer analysis. A global mesh size of 15 mm is used to discrete the rigid plate. The time period of Step 2 is specified as 6300 which corresponds to 105 minutes. In the Step 2, the maximum number of time increments is 500; the initial increment size is 30; and the minimum and maximum increment size is 1×10^{-9} and 300, respectively. The CFS column and rigid plate are modeled with a 4-node shell element with reduced integration (S4R) and rigid bilinear quadrilateral elements (R3D4), respectively.

When it is exposed to the elevated temperature, mechanical properties of steel deteriorate rapidly which consequently reduces the stiffness and strength of the CFS column. The yield strength, elastic modulus and Poisson's ratio of steel at ambient temperature are taken as 345 MPa, 203 GPa and 0.3, respectively. Figure 4 shows the nominal stress-strain relationship of cold-formed steel at elevated temperatures, which is derived base on part 1.2 of Eurocode 3 [13]. Steel expands considerably when exposed to elevated temperatures. Therefore, thermal bowing will be developed due to the presence of non-uniform temperature distributions across the cross-section. Hence, the coefficient of thermal expansion of CFS at different temperature needs to be determined for the structural analysis of CFS wall systems at elevated temperatures. In this study, the coefficient of thermal expansion of CFS stipulated in Eurocode 3 Part 1.2 [13] is adopted, which is the same as that of hot-rolled steel.

Figure 5 illustrates the load and boundary conditions of the modelled CFS column. The column is simply supported with translational displacements, i.e., UX, UY and UZ at the lower end and UX and UY at the upper end are restrained. Twisting about the Z axis (URZ) is restrained at both ends. A target axial load is applied first via the reference node of the rigid plate at the upper end. The load ratio (R), i.e., the ratio of the applied load at the fire limit state and the ultimate compressive strength of the CFS column at ambient temperature, ranges from 0.6 to 0.9. Table 1 shows the applied axial load of CFS C-shape columns in the FE structural model. At ambient temperature, the ultimate compressive strength drops gradually as the perforation length increases. For example, with length of wen perforation L_h=630 mm, the ultimate strength of the CFS C-shape column is only about 60% of that without perforations. Initial

global geometrical imperfection is accounted for through eigenvalue buckling analysis. The first mode shape and a magnitude of one thousandth of the column length (L/1000) is adopted (Figure 6). The time dependent nodal temperatures obtained from the thermal analysis (Figure 3(b)) are incorporated into the structural model as a predefined boundary condition. The ambient temperature of 20 ºC is also adopted.

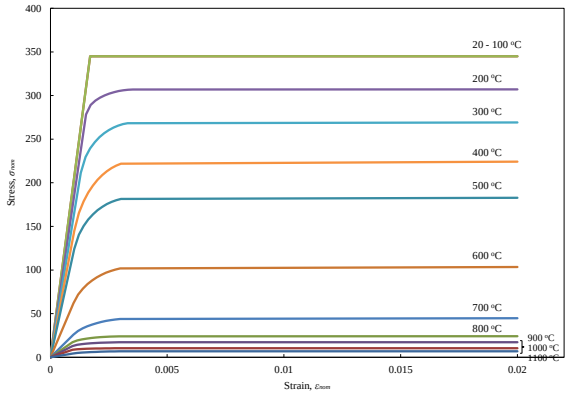

Figure 4 Stress-strain relationship of steel at elevated temperatures

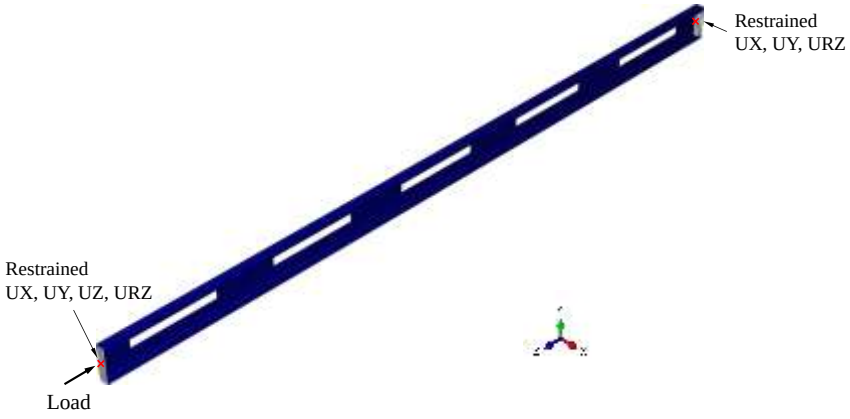

Figure 5 Load and boundary conditions in structural analysis

Table 1 Applied load at ambient temperature (Step-1)

L_h (mm)	Applied load (kN)				
	R=0.9	R=0.8	R=0.7	R=0.6	R=0.5
0	14.8	13.2	11.5	9.9	8.2
130	13.3	11.8	10.3	8.9	7.4
250	12.4	11.1	9.7	8.3	6.9
380	12.1	10.7	9.4	8.0	6.7
510	11.2	10.0	8.7	7.5	6.2
630	9.0	8.0	7.0	6.0	5.0

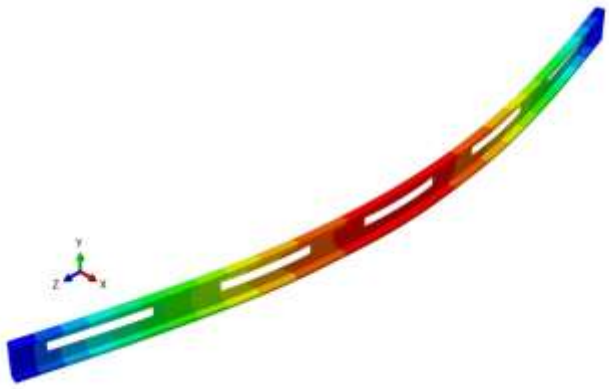

Figure 6 Initial global geometric imperfection (L/1000)

3. Results and discussions

Figure 7 and 8 shows the predicted external reaction force at the lower end and axial deformation of the column at the upper end, respectively, for a CFS C-shape column with the length of web perforation L_h=380 mm (15 in.) and the load ratio R=0.9. As shown in Figure 8, the column shortens initially due to the applied axial load at ambient temperature and then gradually expands as the increase of temperature. However, the magnitude of the external reaction force at the lower end maintains that same as that of applied load until the failure of the column occurs. At 48.9 minutes, the column fails evidenced by the rapid increase column deformation and sudden decrease of the reaction force at the lower end of the column shown in Figure 8. The corresponding end reaction force and axial deformation of the column at the failure is about 85% of the initially applied load and 54 mm, respectively.

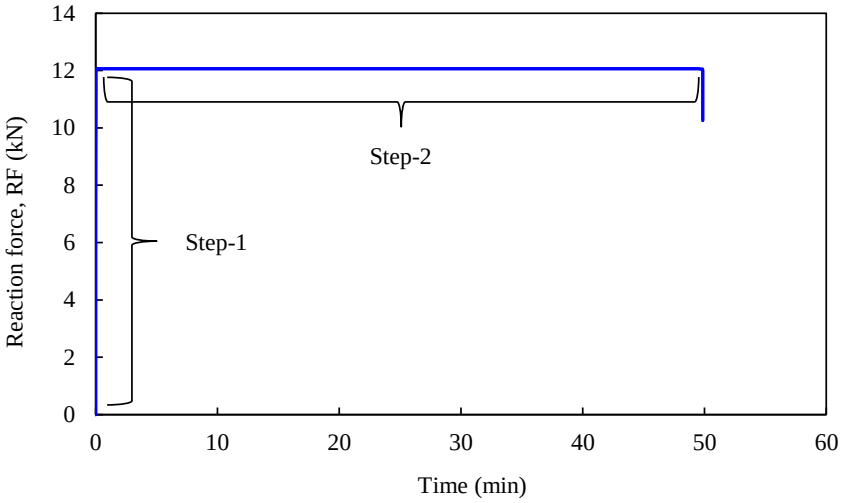

Figure 7 Time-end reaction force curve (L_h=380 mm, R=0.9)

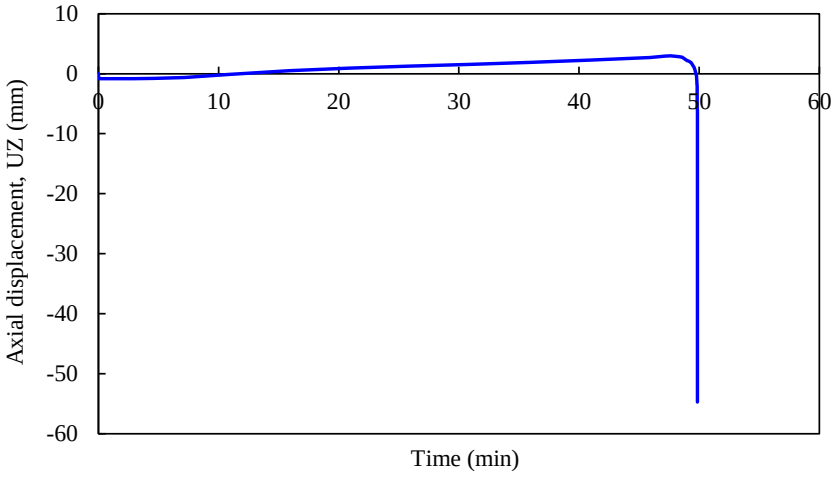

Figure 8 Time-axial deformation curve (L_h=380 mm, R=0.9)

Figure 9 shows the predicted failure mode of the CFS C-shape column with L_h=380 mm (15 in.) and a load ratio of 0.9. Global buckling about Y-axis together with local failure around the perforation at mid-height is observed. No torsional buckling about Z-axis occurs since the rotation URZ is assumed to be restrained by the presence of gypsum board on both flanges of the CFS C-shape columns. Thermal bowing is towards the fire-exposed side. The flange of the column on the fire-exposed side buckles first due to the higher temperature which results rapid degradation on both stiffness and strength of the flange. Consequently, the flange on the fire-unexposed side bears the increasing load and failure subsequently.

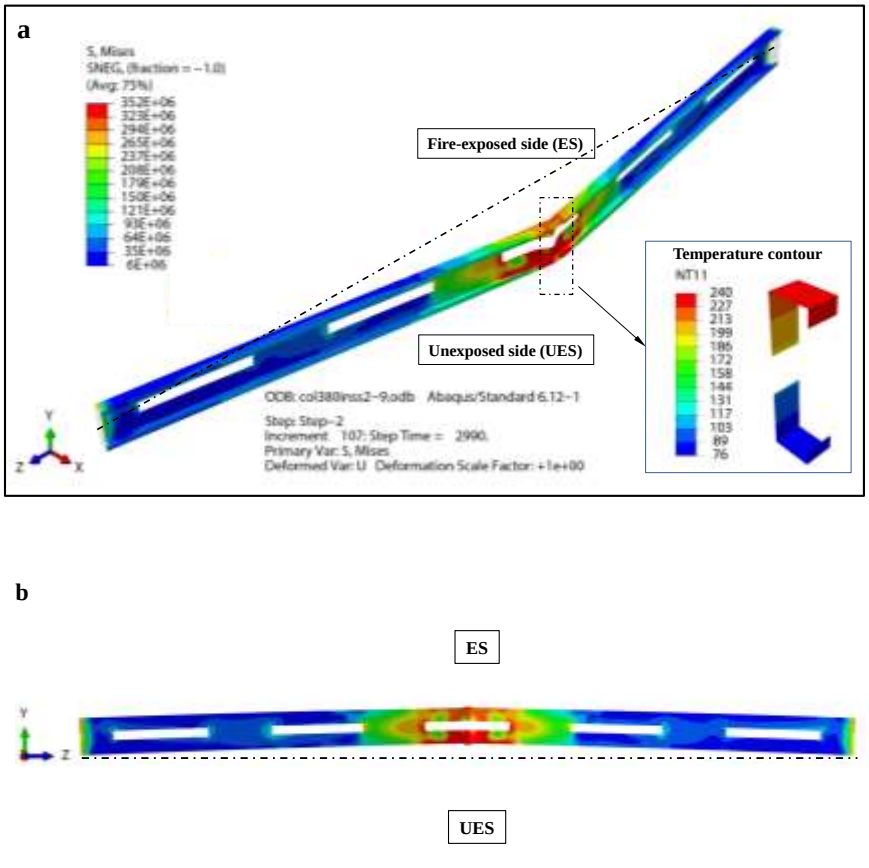

Figure 9 Failure mode (L_h=380 mm, R=0.9): (a) elevation, and (b) YZ plane.

Figure 10 compares the effect of perforation length on the predicted failure time. At a given perforation length, the failure time decreases rapidly as the load ratio increases. For the case of no web perforations i.e., L_h=0 mm, the corresponding failure time is 90.2 minutes for R=0.6, and 48.7 minutes when R=0.9. The failure time of the latter case is about 46% less than that the former one. It is found in this investigation that for a given load ratio, the variation among failure times for columns with different L_h is within 10%, which is not significant.

In addition, for a CFS C-shape column with a specified load ratio, the capacity of the column at elevated temperature are significantly influenced by degradation of material properties of steel and fire exposure time whereas the distribution of non-uniform cross-sectional temperature has a minor influence on the capacity of the column. Figure 11 compares the temperature contour of CFS C-shape columns with different web perforation lengths L_h=0 mm, L_h=380 mm and L_h=630 in the region of mid-height of the columns at the exact failure time. It can be seen from the figure there is a minor variation in temperature distributions among these cross-sections, which provides further explanations for the results presented in Figure 10. The web perforation width investigated in this study maintains a constant of 38 mm (1.5 in.), that is, ¼ of the web depth of 150 mm (6 in.). If the perforation width increases, a larger temperature gradient is expected which may consequently result in a greater influence on the behaviour of the CFS C-shape columns.

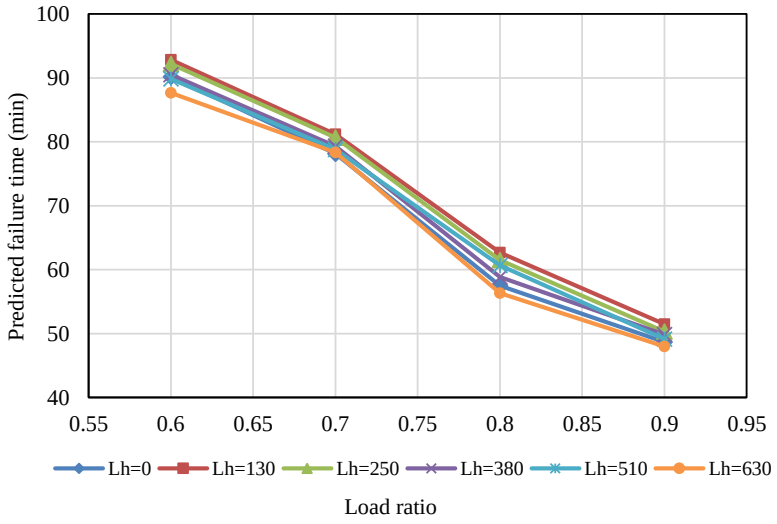

Figure 10 Effect of perforation length on failure time

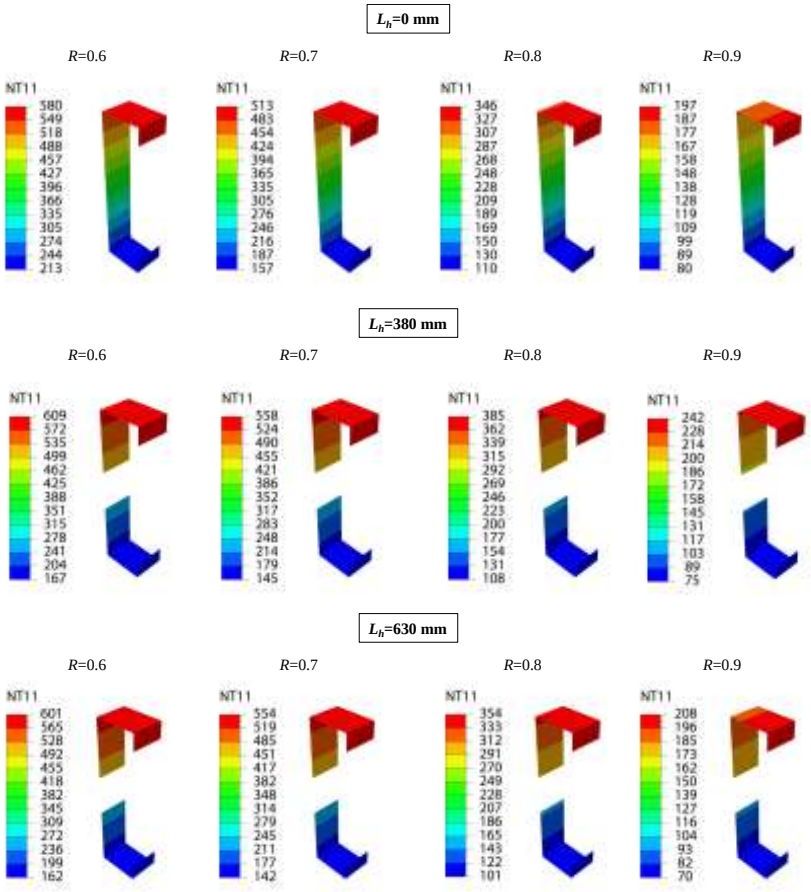

Figure 11 Effect of perforation length on failure mode

4. Conclusions

The effects of web perforations on the behavior of CFS C-shape slender columns subjected to non-uniform cross-sectional distribution of elevated temperatures are investigated in this study. The results from FEA show that perforations in the web can result in a minor increase of temperature gradient within the cross-section of the column. In addition, increase the length of the web perforation does not appear to have a significant influence on the temperature gradient as well. However, the length of web perforation does affect both stiffness and strength of the column at both ambient and elevated

temperatures. At the elevated temperature, the strength of the CFS C-shape columns decreases rapidly as the perforation length increases. However, the length of web perforation appears to have not a significant influence on the failure time as the differences of failure times for the CFS C-shape columns with different perforation lengths investigated in this study are found to be within 10%.

References

1. Feng, M., Wang, Y. C., and Davies, J. M. "Structural behaviour of cold-formed thin-walled short steel channel columns at elevated temperatures. Part 1: experiments." *Thin-walled structures* 41.6 (2003): 543-570.

2. Gunalan, S., Bandula, H., and Mahendran, M. "Local buckling studies of cold-formed steel compression members at elevated temperatures." *Journal of Constructional Steel Research* 108 (2015): 31-45.

3. Thanuja, R., and Mahendran, M. "Distortional buckling tests of cold-formed steel compression members at elevated temperatures." *Journal of Constructional Steel Research* 65.2 (2009): 249-259.

4. Bandula, H., and Mahendran, M. "Flexural-torsional buckling tests of cold-formed steel compression members at elevated temperatures." *Steel and Composite Structures* 14.3 (2013): 205-227.

5. Feng, M., Wang, Y. C., and Davies, J. M. "Structural behaviour of cold-formed thin-walled short steel channel columns at elevated temperatures. Part 2: Design calculations and numerical analysis." *Thin-walled structures* 41.6 (2003): 543-570.

6. Zhao, B., Kruppa, J., Renaud, C., O'Connor, M., Mecozzi, E., Apiazu, W., and Salmi, P. 2005. "Calculation rules of lightweight steel sections in fire situations," France: European Communities.

7. Gunalan, S., & Mahendran, M. 2013. "Finite element modelling of load bearing cold-formed steel wall systems under fire conditions," *Engineering Structures* 56, 1007-1027.

8. Yang S., & Xu, L. 2016. "3D FEA of load-bearing cold-formed steel wall systems with web-perforated studs subjected to standard fire", *Proceeding of 9th international conference on structures in fire*, Jun. 8-10, 2016. Princeton, New Jersey, United States.

9. Shahbazian, A., and Wang, Y. C. "Calculating the global buckling resistance of thin-walled steel members with uniform and non-uniform elevated temperatures under axial compression." *Thin-Walled Structures* 49.11 (2011): 1415-1428.

10. HKS, ABAQUS Standard User's Manual Version 6.12, Hibbit, Karlsson & Sorensen Inc., USA, 2012.

11. Keerthan, P., & Mahendran, M. 2012. "Numerical modelling of non-load-bearing light gauge cold-formed steel frame walls under fire conditions," *Journal of Fire Sciences* 0(0) 1-29.

12. ISO 834-1 1999. "Fire resistance tests – elements of building construction - Part 1: general requirements," International Organization for Standardization, Geneva, Switzerland.

13. Eurocode 3. 2005. "EN1993-1-2: The European Standard; Part 1-2: General rules - Structural fire design," European Committee for Standardization, Brussels, Belgium.